Optics Communications 284 (2011) 2027–2030

Contents lists available at ScienceDirect

Optics Communications

journal homepage: www.elsevier.com/locate/optcom

Investigation of symmetries of second-order nonlinear susceptibility tensor of GaSe crystals in THz domain

Guibao Xu [a], Guan Sun [a], Yujie J. Ding [a,*], Ioulia B. Zotova [b], Krishna C. Mandal [e], Alket Mertiri [c], Gary Pabst [c], Nils Fernelius [d]

[a] Department of Electrical and Computer Engineering, Lehigh University, Bethlehem, PA 18015, USA
[b] ArkLight, P.O. Box 2, Center Valley, PA 18034, USA
[c] EIC Laboratories, Inc., Norwood, MA 02062, USA
[d] Materials and Manufacturing Directorate, Air Force Research Laboratory, Wright-Patterson AFB, OH 45433, USA
[e] Department of Electrical Engineering, University of South Carolina, Columbia, SC 29208, USA

ARTICLE INFO

Article history:
Received 23 October 2010
Received in revised form 7 December 2010
Accepted 7 December 2010
Available online 22 December 2010

Keywords:
Kleinman's symmetry condition
Spatial symmetry
THz generation
GaSe
Optical rectification
Photocurrent surge

ABSTRACT

Following our measurements and analysis made on several GaSe crystals, we demonstrated that terahertz (THz) generation from ultrafast laser pulses can be developed into a sensitive technique for investigating symmetries of second-order nonlinear susceptibility tensor of a nonlinear crystal. Indeed, for GaSe crystals, both Kleinman's symmetry condition and spatial symmetry were violated due to the contribution of ionic displacement to nonlinear polarization and deviation of GaSe lattice from hexagonal symmetry. When the pump photon energy was increased from that below the bandgap of GaSe to that above it, the mechanism for the THz generation was switched from optical rectification to photocurrent surge.

1. Introduction

Terahertz (THz) waves have important applications in spectroscopic analysis of chemicals [1], pollution monitoring [2], nondestructive evaluation [3], detections and identifications of explosives [4], far-field imaging [5], remote sensing [6], and biomedical diagnostics [7]. Among different methods used for THz generation, generation by ultrafast laser pulses has an advantage for producing extremely high peak-power broadband THz pulses [8]. According to our previous studies [9], GaSe ranked the third in terms of the average THz output powers generated by ultrafast laser pulses. Besides generation, it can be used in ultrabroadband THz detection in time-domain spectroscopy [10,11]. On the other hand, it was demonstrated that GaSe can be used for efficient generation of monochromatic THz radiation tunable in an extremely-wide frequency range [12,13].

In almost all the previous works [10–13], the THz generation and detection in GaSe crystals is attributed to optical rectification based on second-order nonlinearities. Since the symmetries of the second-order nonlinear susceptibility tensor affect the effective second-order nonlinear coefficient, they may also affect the THz generation and detection. In particular, Kleinman's symmetry condition and spatial symmetry have been applied, in order to simply certain elements of the second-order nonlinear susceptibility tensor for GaSe having point group 62m. However, the detailed study on whether these two symmetry conditions are valid has not been carried out. In the past, by measuring the THz electric field as a function of azimuth angle, the ratios between nonlinear optical coefficients were determined based on electro-optic sampling [14,15].

In this article, we demonstrate that the ratios between the elements of second-order nonlinear susceptibility tensor for GaSe crystals can be readily deduced by monitoring characteristics of the THz output power. Following our result and analysis, we conclude that both Kleinman's symmetry condition and spatial symmetry are violated for THz generation.

2. GaSe crystals and experimental condition

GaSe crystals in our experiment were grown by a Bridgman method. During the crystal growth, In or Cr was introduced as a dopant to replace Ga in order to improve the crystal hardness [16]. Each sample has two facets perpendicular to the *c* axis being separated about 1 mm. The doping level and crystal thickness of our GaSe crystals are listed in Table 1.

* Corresponding author.
E-mail address: yud2@lehigh.edu (Y.J. Ding).

0030-4018/$ – see front matter © 2010 Elsevier B.V. All rights reserved.
doi:10.1016/j.optcom.2010.12.025

Table 1
Summary of data on GaSe crystals. Excitation wavelengths: * — 782 nm, † — 391 nm.

Sample	Thickness (mm)	Dopant (ppm)	d_{16}/d_{21}	d_{22}/d_{21}	Highest Output Power	
					P1* (μW)	P2† (μW)
GSU0145	0.15	Undoped	0.873	−1.068	5.470	–
GSU7903	1.0	Undoped	0.979	−1.042	19.405	0.060
GSI8701	1.0	In (500)	1.004	−1.063	22.929	0.037
GSI7801	0.9	In (3000)	–	–	16.332	0.043
GSC8902	1.1	Cr (500)	–	–	19.451	0.037

Broadband THz pulses were generated from these crystals by using a Ti:sapphire regenerative amplifier at the center wavelength of 782 nm and a coherent beam at the center wavelength of 391 nm obtained after frequency-doubling of the Ti:sapphire laser beam in a BBO crystal. The pulse width and repetition rate for both of the coherent beams are 180 fs and 250 kHz, respectively. After each excitation beam was focused onto one of the crystal facets, the THz radiation beam was collimated and then focused to a pyroelectric detector for measuring the THz output powers in the transmission and reflection geometries.

3. Results and analysis

The highest output powers generated from different GaSe crystals in our experiment are summarized in Table 1. At the average pump power of 1.14 W at 782 nm, the THz output powers were measured to be in the range of 16.3–22.9 μW from four GaSe crystals in the transmission geometry. Among different GaSe samples, the highest output power is 23 μW. This is amounted to an improvement by a factor of 4.2 compared to our previous result on GaSe [9]. Such an enhancement is caused by the combination between the linear scaling of the output power with the interaction length and phase-mismatch factor when the interaction length is comparable to the coherence lengths [9]. After normalizing the highest THz output power by the crystal thickness for the four bulk GaSe crystals (i.e. the bottom four in Table 1), the normalized output power is improved by introducing a small amount (500 ppm) of In. This increase may be caused by the increase in the effective second-order nonlinear coefficient, which is consistent with the previous report [17]. However, based on our result, crystal quality may be deteriorated after introducing Cr at the level of 500 ppm. This could be attributed to the increase in the density of the defects, resulting in the increase in the absorption of the THz wave. It is worth noting that due to the phase-mismatch factor, as mentioned above, the four crystals do not scale down linearly with the interaction length, when being compared with the 0.15-mm-thickness crystal.

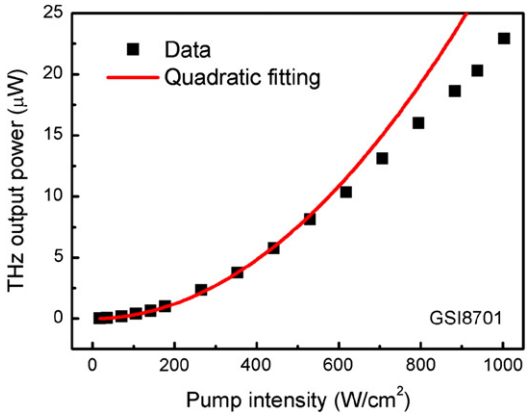

Fig. 1. Average THz output power as a function of average pump intensity for GaSe crystal GSI8701. The excitation wavelength is 782 nm. Squares correspond to the experimental data. Solid curve corresponds to the quadratic least-square fitting to nine data points from the low-intensity end.

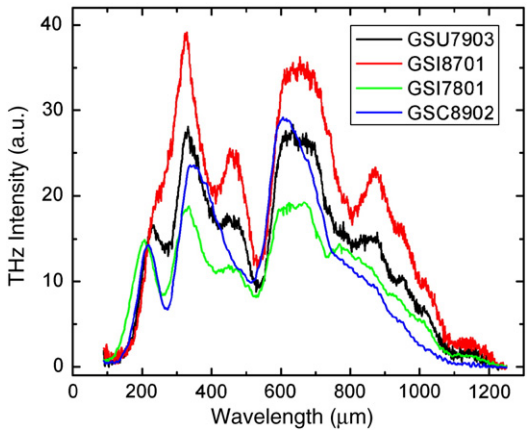

Fig. 2. Spectra of THz waves emitted from GaSe crystals under pump wavelength of 782 nm and pump intensity of 1003 W/cm^2.

According to Fig. 1, when the pump intensity is lower than 618 W/cm^2, the power dependence for crystal GSI8701 is well fitted by a square power law. However, for the pump intensity of above 618 W/cm^2, the power dependence is below the quadratic power law. We have noticed similar behaviors for all four GaSe crystals. Due to the strong two-photon absorption [18] at extremely-high peak intensities of the pump beam (e.g. 13.7 GW/cm^2 corresponding to the average pump intensity 618 W/cm^2), the power dependence significantly deviated from the quadratic power law. In addition, the two-photon-absorption-induced free carriers in GaSe crystal may absorb the THz radiation, resulting in the effective decrease of the THz output power [19,20]. The spectra of THz radiation measured on GaSe crystals by rotating a mechanical THz grating are illustrated in Fig. 2. We can see that the THz spectra from different samples are very similar, covering the wavelength range from 150 μm to 1200 μm (i.e. the frequency range from 250 GHz to 2 THz). The obvious modulations appearing in the THz spectra, located at around 273 μm, 407 μm, 538 μm and 802 μm, respectively, are attributed to water vapor absorption after comparing them with the resonance frequencies of the water vapor available at Hitran database [21].

It is worth noting that optical rectification of ultrafast pulses is a second-order nonlinear process. For GaSe, the second-order nonlinear susceptibility tensor has three nonzero elements due to its structural symmetry, and therefore, the nonlinear polarization at the THz frequency can be derived from the following matrix product:

$$\begin{pmatrix} P_x^{THz} \\ P_y^{THz} \\ P_z^{THz} \end{pmatrix} = \begin{pmatrix} 0 & 0 & 0 & 0 & 0 & d_{16} \\ d_{21} & d_{22} & 0 & 0 & 0 & 0 \\ 0 & 0 & 0 & 0 & 0 & 0 \end{pmatrix} \begin{pmatrix} E_x^2 \\ E_y^2 \\ E_z^2 \\ 2E_yE_z \\ 2E_zE_x \\ 2E_xE_y \end{pmatrix} \quad (1)$$

Under the normal incidence for the pump laser beam, the components of the nonlinear polarization at the THz frequency, generated by GaSe, are given by

$$P_x = 4d_{16}E_xE_y; \qquad P_y = 2d_{21}E_x^2 + 2d_{22}E_y^2 \quad (2)$$

where $E_x = E_0\cos\theta$ and $E_y = E_0\sin\theta$ are projections of the pump polarization (E_0) onto x and y axes, respectively, and θ is the

polarization angle of the pump beam being defined relative to the x axis.

When both Kleinman's symmetry condition ($d_{16}=d_{21}$) and spatial symmetry ($d_{22}=-d_{21}$) are satisfied, the second-order nonlinear susceptibility tensor of GaSe has only one nonzero independent element. Therefore, the magnitude and angle of the nonlinear polarization at the THz frequency can be derived from Eq. (2) as:

$$P_{THz}=\sqrt{P_x^2+P_y^2}=2d_{22}E_0^2 \tag{3}$$

$$\theta_{THz}=\tan^{-1}\left(\frac{P_y}{P_x}\right)=\frac{3}{2}\pi-2\theta. \tag{4}$$

Since the intensity of the THz output is proportional to the square of P_{THz}, it is independent of the polarization angle of the pump beam whereas the polarization angle of the THz output is linearly dependent on the polarization angle of the pump beam. However, such a predicted behavior of the THz output power vs. the pump polarization angle is inconsistent with our experimental results, see Figs. 3 and 4. Indeed, for two GaSe crystals, the measured dependence of the THz output power on the pump polarization angle exhibited periodic oscillations instead of constants, see Figs. 3 and 4.

Our closer examination of Kleinman's symmetry condition reveals that it is valid only for a lossless medium in which case the dispersion of second-order nonlinear susceptibility is negligible. If one of the frequencies for the waves participating in the parametric interaction is below the ionic resonance frequencies, both electronic and ionic displacements contribute to the nonlinear polarization, and therefore, the second-order nonlinear susceptibility becomes frequency-dependent. For GaSe, one of the ionic resonance frequencies is 6.41 THz (the corresponding wavelength of 46.8 μm) for the transverse-optical (TO) phonon frequency, which is significantly higher than the THz frequencies generated by us, see Fig. 2. Therefore, the second-order nonlinear susceptibility for GaSe depends on the THz frequency. This implies that the Kleinman's symmetry condition is violated for the THz generation. In addition, GaSe is well known for its layer structure. Indeed, each layer consists of four two-dimensional atomic sheets, with the sequence of Se–Ga–Ga–Se, bounded together by strong forces, mostly covalent. However, the forces between layers belong to the weak van der Waals type. The layer structure for GaSe at room temperature has the hexagonal symmetry (ε-GaSe), which results in the spatial symmetry condition, i.e. $d_{22}=-d_{21}$. However, due to the strain induced by imperfection or doping in crystal growth, the rather

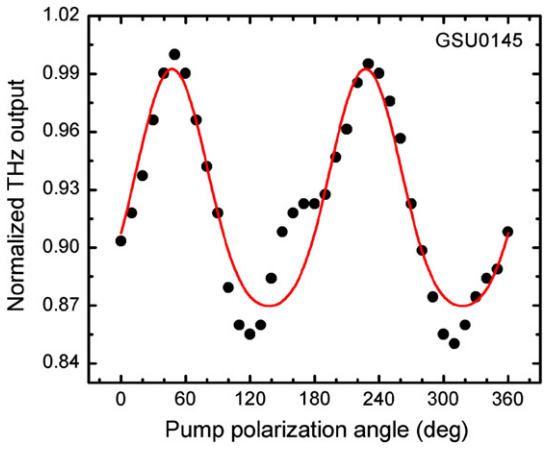

Fig. 3. Normalized THz output power as a function of pump polarization angle with pump wavelength of 782 nm for GaSe film GSU0145. Dots correspond to experimental data. Solid curve corresponds to the nonlinear least-square fitting by using Eq. (5).

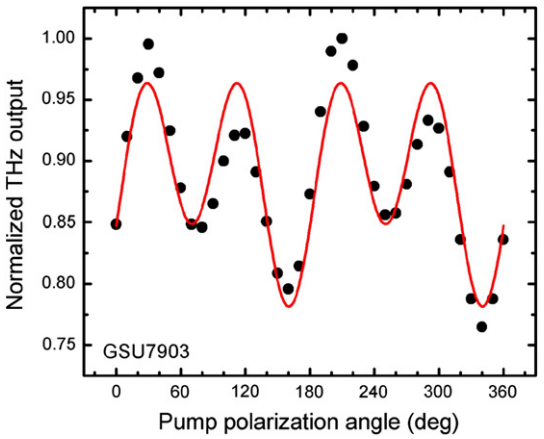

Fig. 4. Normalized THz output power as a function of pump polarization angle with pump wavelength of 782 nm for GaSe crystal GSU7903. Dots correspond to experimental data. Solid curve corresponds to the nonlinear least-square fitting by using Eq. (5).

flexible layer structure of GaSe may deviate from its perfect hexagonal symmetry. As a result, the spatial symmetry condition of $d_{22}=-d_{21}$ is no longer valid.

When both Kleinman's symmetry condition and spatial symmetry are no longer valid, we have obtained the expressions for the amplitude and angle of the nonlinear polarization at the THz frequency:

$$P_T=d_{22}E_0^2\sqrt{4\left(\frac{d_{16}}{d_{22}}\right)^2\sin^2(2\theta)+2\left(\frac{d_{21}}{d_{22}}\right)\sin^2(2\theta)+4\left(\frac{d_{21}}{d_{22}}\right)^2\cos^4\theta+4\sin^4\theta} \tag{5}$$

$$\theta_T=\tan^{-1}\left[\frac{(d_{21}/d_{22})\cos^2\theta+\sin^2\theta}{(d_{16}/d_{22})\sin(2\theta)}\right]. \tag{6}$$

By varying the ratios of d_{16}/d_{22} and d_{21}/d_{22}, we have achieved the nonlinear-least-square fit to the data of the THz output power vs. pump polarization angle by using Eq. (5), see Figs. 3 and 4. Specifically, we first estimated an approximate value for d_{16}/d_{21}. This can be done by assuming that the ratio of d_{21}/d_{22} is exactly -1, while deducing the ratio of d_{16}/d_{21} through the nonlinear-least-square fit to the data points. Subsequently, we simultaneously deduced the ratios of d_{21}/d_{22} and d_{16}/d_{21} through the nonlinear-least-square fit to the data points by using the pair of the values above as the initial values. Consequently, we have obtained the optimal values for d_{16}/d_{22} and d_{21}/d_{22} for three samples, see Table 1. According to Table 1, the ratios between d_{16} and d_{21} are different among three samples by at most 14%. In contrast, the ratios between d_{22} and d_{21} vary only by 2.5%. However, according to Fig. 5, the ratios of d_{16}/d_{22} and d_{21}/d_{22} have a negligible effect on the THz polarization angle vs. the pump polarization angle, due to the strong linear dependence, which has completely masked the slight deviations of the THz polarization angle vs. the pump polarization from the linear behavior. We would like to mention that for the last two samples listed in Table 1, we were not able to deduce the ratios due to the damage occurred to the crystals during the experiment.

When the GaSe crystals were pumped above the bandgap of GaSe by using a coherent beam at 391 nm obtained by frequency-doubling in a BBO crystal, the THz output powers were measured under the reflection geometry at an incident angle of 71° for the pump beam, i.e. the Brewster angle for the pump beam,. The output powers were reduced by two orders of magnitude, see Table 1. In the past, it was demonstrated that both optical rectification and photocurrent surge contribute to the THz generation, when the pump photon energy was

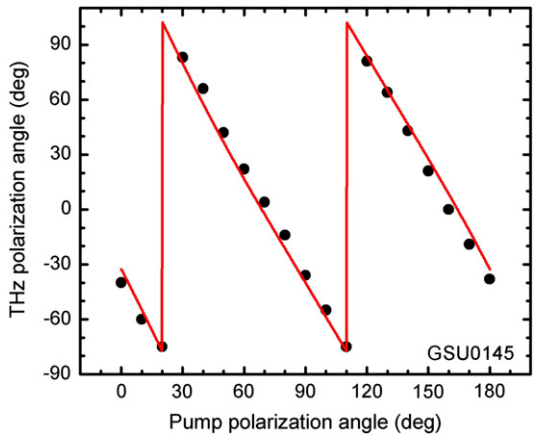

Fig. 5. Typical polarization angle of THz beam as a function of pump polarization angle with pump wavelength of 782 nm. Dots correspond to experimental data. Solid curve corresponds to the nonlinear least-square fitting by using Eq. (6).

set above the bandgap in InN [20] and InAs [22], respectively. However, for the GaSe crystals, the THz generation from GaSe crystals exhibited the typical behavior originating from photocurrent surge. One can see from Fig. 6(a) and (b) that at an incident angle of 71° the polarization angle for the THz output beam was more or less a constant regardless of what the pump polarization angle or azimuth angle was. Such behaviors are clear indications that the mechanism for the THz generation pumped at 391 nm was induced by photocurrent surge. On the other hand, the dependence of the THz output power on the pump polarization angle exhibited an oscillation over two periods within 0–360°, which can be well fitted after taking into consideration the Fresnel reflection of the pump beam at the crystal entrance facets, see the solid curve in Fig. 6(a). Such a behavior can be used to rule out the contribution of the optical rectification to the THz generation.

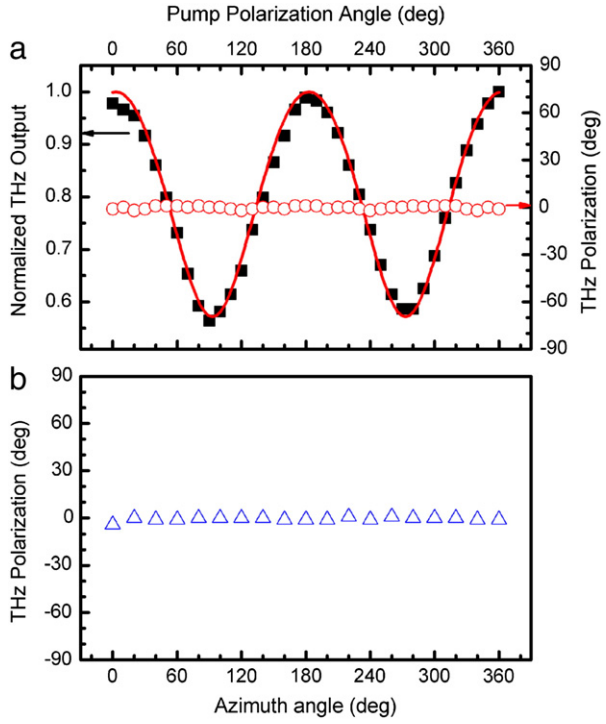

Fig. 6. Typical (a) polarization dependence and (b) azimuth angle dependence of GaSe crystal with the pump wavelength of 391 nm in reflection scheme. Squares and circles are the measured output power and polarization angle of THz beam, respectively, versus the pump polarization. Solid curve is the theoretical result after taking into consideration Fresnel reflections at crystal/air surface. And up-triangles are the measured THz polarization angle as a function of crystal azimuth angle.

4. Concluding remarks

By using the GaSe crystals, we demonstrated that both the Kleinman's symmetry condition and spatial symmetry were violated for the THz generation. The violation of the Kleinman's symmetry condition was caused by the contribution of the ionic displacement to the nonlinear polarization since the THz output frequencies were below the ionic resonance frequencies. On the other hand, the violation of the spatial symmetry reflected the deviation of the GaSe lattice from the hexagonal symmetry due to the rather flexible layer-stacking structure for GaSe. By fitting the THz output power as a function of the pump polarization angle, the ratios between the elements of second-order nonlinear susceptibility tensor, i.e. d_{16}/d_{21} and d_{22}/d_{21}, can be deduced. Therefore, we conclude that the THz output power vs. the pump polarization angle can be developed into a sensitive technique for investigating the symmetries of the second-order nonlinear susceptibility tensor of a nonlinear crystal. When the pump photon energy was increased from that below the bandgap to that above the bandgap of GaSe, the mechanism for the THz generation was switched from optical rectification to photocurrent surge.

Acknowledgement

This work has been supported by the U.S. Air Force Research Laboratory.

References

[1] H. Sun, Y.J. Ding, I.B. Zotova, IEEE Sensors J. 10 (2010) 621.
[2] J.W. Waters, IEEE Trans. Geosci. Remote Sens. 44 (2006) 1075.
[3] H. Zhong, J. Xu, X. Xie, T. Yuan, R. Reightler, E. Madaras, X.-C. Zhang, IEEE Sensors J. 5 (2005) 203.
[4] H.-B. Liu, Y. Chen, G.J. Bastiaans, X.-C. Zhang, Opt. Express 14 (2006) 415.
[5] T. Yasuda, T. Yasui, T. Araki, E. Abraham, Opt. Commun. 267 (2006) 128.
[6] J. Liu, J. Dai, S.L. Chin, X.-C. Zhang, Nat. Photonics 4 (2010) 627.
[7] R.M. Woodward, B.E. Cole, V.P. Wallace, R.J. Pye, D.d. Arnone, E.H. Linfield, M. Pepper, Phys. Med. Biol. 47 (2002) 3853.
[8] F. Blanchard, L. Razzari, H.-C. Bandulet, G. Sharma, R. Morandotti, J.-C. Kieffer, T. Ozaki, M. Reid, H.F. Tiedje, H.K. Haugen, F.A. Hegmann, Opt. Express 15 (2007) 13212.
[9] X. Mu, I.B. Zotova, Y.J. Ding, IEEE J. Sel. Top. Quantum Electron. 14 (2008) 315.
[10] K. Liu, J. Zhou, X.-C. Zhang, Appl. Phys. Lett. 85 (2004) 863.
[11] C. Kübler, R. Huber, S. Tübel, A. Leitenstorfer, Appl. Phys. Lett. 85 (2004) 3360.
[12] W. Shi, Y.J. Ding, N. Fernelius, K. Vodopyanov, Opt. Lett. 27 (2002) 1454.
[13] W. Shi, Y.J. Ding, Appl. Phys. Lett. 84 (2004) 1635.
[14] X.-C. Zhang, Y. Jin, X.F. Ma, Appl. Phys. Lett. 61 (1992) 2764.
[15] X.-C. Zhang, X.F. Ma, Y. Jin, T.-M. Lu, E.P. Boden, P.D. Phelps, K.R. Stewart, C.P. Yakymyshyn, Appl. Phys. Lett. 61 (1992) 3080.
[16] V.G. Voevodin, O.V. Voevodina, S.A. Bereznaya, Z.V. Korotchenko, A.N. Morozov, S. Y. Sarkisov, N.C. Fernelius, J.T. Goldstein, Opt. Mater. 26 (2004) 495.
[17] D.R. Suhre, N.B. Singh, V. Balakrishna, N.C. Fernelius, F.K. Hopkins, Opt. Lett. 22 (1997) 775.
[18] I.B. Zotova, Y.J. Ding, Appl. Opt. 40 (2001) 6654.
[19] Y.J. Ding, IEEE J. Sel. Top. Quantum Electron. 10 (2004) 1171.
[20] G. Xu, Y.J. Ding, H. Zhao, G. Liu, M. Jamil, N. Tansu, I.B. Zotova, C.E. Stutz, D.E. Diggs, N. Fernelius, F.K. Hopkins, C.S. Gallinat, G. Koblmüller, J.S. Speck, Semicond. Sci. Technol. 25 (2010) 015004.
[21] http://www.cfa.harvard.edu/HITRAN/.
[22] X. Mu, Y.J. Ding, Y.B. Zotova, Opt. Lett. 32 (2007) 3321.